AIAA JOURNAL
Vol. 47, No. 4, April 2009

Accurate and Robust Pressure Weight Advection Upstream Splitting Method for Magnetohydrodynamics Equations

Sang-Hoon Han,* Jeong-Il Lee,† and Kyu Hong Kim‡
Seoul National University, Seoul 151-742, Republic of Korea

DOI: 10.2514/1.39375

Two variants of the advection upstream splitting method are modified to solve the equations of ideal magnetohydrodynamics. Discontinuity-sensing functions used in AUSMPW+ and M-AUSMPW+ for the magnetohydrodynamics equations are newly defined in consideration of a magnetic field. The new pressure-based weight functions are shown to effectively remove the oscillations behind a strong shock wave as well as provide a highly accurate solution for a stationary contact discontinuity. To satisfy the divergence-free constraint of a magnetic field, the hyperbolic divergence cleaning method is chosen and applied for all the test cases. Ryu and Jones' one-dimensional magnetohydrodynamics shock-tube problem and Orszag and Tang's two-dimensional magnetohydrodynamics vortex system are evaluated to validate and show the advantages of the newly developed schemes.

Nomenclature

B_x, B_y, B_z	=	magnetic field components in the x, y, and z
c	=	speed of sound
c_a	=	speed of Alfvén wave
c_f	=	speed of fast magnetosonic wave
c_h	=	speed of transporting divergence errors
c_p	=	dissipative parameter of hyperbolic divergence cleaning method
c_s	=	speed of slow magnetosonic wave
e	=	specific total energy
F	=	flux vector components in x direction
G	=	flux vector components in y direction
M	=	Mach number
p	=	pressure
U	=	conservative variable vector
u, v, w	=	velocity components in the x, y and z directions
x, y	=	Cartesian coordinates
γ	=	ratio of specific heats
λ	=	eigenvalue
ρ	=	density
$\mathbf{\Phi}$	=	convective properties of advection upstream splitting method
ψ	=	Lagrange multiplier

I. Introduction

OVER the past few decades, researchers have shown much interest in magnetohydrodynamics (MHD) because of its many possible applications to astrophysics, geophysics, thermonuclear engineering, electrical engineering, aerospace engineering, and so on. Because the MHD equations basically consist of a nonlinear system of equations of fluid dynamics and electrodynamics, they require the understanding of complex multiphysics. To formulate a numerical scheme for solving the MHD equations, Yee [1] applied the staggered grid (Yee grid) method to solve the Maxwell equations for an electromagnetic field, and this method has been widely used to clean the divergence errors of the MHD equations [2–4]. In the thermonuclear and fusion fields, various finite element methods such as NIMROD have been used to analyze MHD flows, and they are considered appropriate methods for low-speed flow applications [5–7]. On the other hand, in astrophysics and aerospace engineering, many applications are characterized by high flow velocity as well as shock waves. Thus, a numerical method for such MHD applications should be able to handle discontinuities accurately and stably. For stable shock capturing, many numerical schemes have been developed in gas dynamics. Recently, upwind-type schemes have been recognized to be the most proper scheme for shock capturing. In this respect, upwind-type schemes are more effective in calculating high-speed MHD applications than central differencing schemes.

In 1988, a Roe-type linearized Riemann solver was applied to the MHD equations with the constant $\gamma = 2$ by Brio and Wu [8]. After that, other researchers, including Ryu and Jones [9], Balsara [10], Dai and Woodward [11], Zachary et al [12], Aslan [13], and Harada et al. [14], have used a linearized Riemann solver to solve the MHD equations. Specifically, Balsara [10] and Cargo and Gallice [15] pursued the construction of a Roe-type matrix and the corresponding Roe-type averages to apply for arbitrary γ. Recently, Rossmanith [16,17] successfully analyzed the ideal MHD equations using the wave propagation method, which is a kind of linearized Riemann solver. Basically, linearized Riemann solvers are more accurate than other upwind-type schemes [Steger and Warming [18], van Leer [19], and Harten, Lax, and van Leer (HLL) type] because these solvers can consider all MHD waves physically by using corresponding eigenvalues [20]. However, they require more computational time for the eigen decomposition of the MHD system, especially for multidimensional applications.

As an approximate Riemann solver, the HLL method was generalized to the MHD equations [21]. However, this method showed a smeared result in the contact wave similar to that in gas dynamics because it had no way to recognize the existence of the discontinuity. In addition, it could not accurately resolve the Alfvén wave and slow shock discontinuity. To increase the accuracy for a contact wave, Linde [22] proposed a corrected HLL method, which included the information of contact discontinuity. This method, however, lost the positivity characteristic of the HLL-type schemes for some cases. Similar to Linde's approach, Gurski's approach [23] extended the HLLC (Harten, Lax, and van Leer with contact restoration) Riemann solver of Euler equations to MHD equations and proposed an HLLC-type MHD Riemann solver, which was named smooth HLLC. Li [24] also presented another form of an HLLC-type solver for MHD equations. Unfortunately, these

Received 26 June 2008; revision received 26 December 2008; accepted for publication 28 December 2008.

*Graduate Research Assistant, School of Mechanical and Aerospace Engineering, Sillim-Dong, Gwanak-Gu; airshhan@snu.ac.kr. Member AIAA.

†Postdoctoral Fellow, School of Mechanical and Aerospace Engineering, Sillim-Dong, Gwanak-Gu; snow0730@empal.com. Member AIAA.

‡Assistant Professor, School of Mechanical and Aerospace Engineering and Institute of Advanced Aerospace Technology, Sillim-Dong, Gwanak-Gu; aerocfd1@snu.ac.kr (Corresponding Author). Member AIAA.

HLLC-type solvers had difficulty in resolving Alfvén waves because they had no information about them. Recently, to resolve Alfvén waves accurately using an HLLC solver, Miyoshi and Kusano [25] proposed an HLLD (Harten, Lax, and van Leer discontinuities) solver that had four intermediate states in the Riemann fan.

As another representative upwind scheme, there is the flux vector splitting (FVS) method, such as the van Leer and Steger–Warming schemes. Unfortunately, the Steger–Warming method cannot be applied directly to ideal MHD equations because it is not homogeneous of degree one with respect to the state vector [26]. To apply this method to MHD equations, MacCormack [26] modified the MHD equations into a conservative form of degree-one homogeneity by adopting Powell's model and then used the modified Steger–Warming flux-splitting algorithm to solve them. Shang et al. [27] analyzed the hypersonic blunt body problem using MacComack's modified Steger–Warming scheme. Although this method kept the robustness in capturing the fast shock wave, it had a basic problem: it could not capture the contact discontinuity accurately.

As a hybrid scheme having the advantages of both FDS (flux difference splitting) and FVS (flux vector splitting), AUSM-(advection upstream splitting method) type methods were developed for gas dynamics [28]. The AUSM-type schemes promised an enhanced accuracy over FVS for capturing the contact wave and offered simpler implementation than the linearized Riemann solver like Roe's FDS [28]. In a study related to AUSM-type schemes for MHD equations, Agarwal and Augustinus [29] first applied the original AUSM method with first-order spatial accuracy to one-dimensional cases. Even though it was successfully applied, the AUSM scheme showed a numerical overshoot at a strong shock region and also generated a relatively more diffusive result at a contact discontinuity than a linearized Riemann solver. This was an interesting result because AUSM has been known as a numerical scheme that can capture a contact discontinuity accurately in gas dynamics [28].

No perfect spatial discretized scheme showing accuracy, robustness, and efficiency simultaneously for MHD equations has been developed. Linearized Riemann solvers such as Roe's FDS may provide more accurate results than FVS, HLL, and AUSM-type schemes. However, they require highly expensive computational cost, especially in multidimensional cases. Although FVS, HLL, and AUSM-type schemes are highly efficient, FVS and HLL schemes have accuracy problems in resolving waves other than a fast shock wave, and AUSM-type schemes show an oscillatory behavior in a strong shock wave. Therefore, the goal of the present paper is to develop a new spatial discretization scheme, which can provide higher efficiency than a linearized Riemann solver while retaining stable shock-capturing ability of the FVS and the accuracy level of a linearized Riemann solver. AUSMPW+ [30] and M-AUSMPW+ [31] schemes were chosen as the base flux functions and modified for the ideal MHD calculations.

The contents of this paper are as follows. In Sec. II, the governing equations are presented. In Sec. III, a brief explanation of AUSMPW + /M-AUSMPW+ schemes for gas dynamics are presented. The new discontinuity-sensing terms are introduced for use in the elimination of the oscillations in MHD waves and the modified AUSMPW + /M-AUSMPW+ schemes for the ideal MHD equations are presented. In Sec. IV, numerical tests of the modified AUSMPW+ and M-AUSMPW+ schemes for the two-dimensional Orszag–Tang vortex problem are presented, and concluding remarks are drawn.

II. Governing Equations

Generally, the ideal MHD equations include the continuity, the momentum, the energy, and the magnetic induction equations, and there are no magnetic sources in a magnetic field, that is, a magnetic field has to satisfy the following divergence constraint:

$$\nabla \cdot \mathbf{B} = 0 \tag{1}$$

Across a shock wave, however, it is difficult to satisfy the divergence-free constraint in multidimensions [16]. The violation of the divergence constraint is due to the nonphysical intermediate state within a numerical shock profile. Because this violation may frequently lead to severe stability problems, researchers have tried to enforce the divergence-free constraint in their MHD formulations such as the projection method [32,33], constraint transport method [2–4,16,17,32], eight-wave solution method [32,34], and hyperbolic divergence cleaning method [35–37]. In the present study, the mixed-type hyperbolic divergence cleaning method (HDCM) by Dedner [37] was chosen to eliminate divergence errors because it can be easily implemented without a great modification of the numerical solver. The modified governing equations of the mixed-type HDCM can be written as follows:

$$\frac{\partial U}{\partial t} + \frac{\partial F}{\partial x} + \frac{\partial G}{\partial y} = -H \tag{2}$$

$$U = \begin{bmatrix} \rho \\ \rho u \\ \rho v \\ \rho w \\ B_x \\ B_y \\ B_z \\ \rho e \\ \psi \end{bmatrix}, \quad F = \begin{bmatrix} \rho u \\ \rho u^2 + p_t - B_x^2 \\ \rho v u - B_x B_y \\ \rho w u - B_x B_z \\ \psi \\ B_y u - B_x v \\ B_z u - B_x w \\ (\rho e + p_t) u - B_x (\mathbf{V} \cdot \mathbf{B}) \\ c_h^2 B_x \end{bmatrix}$$

$$G = \begin{bmatrix} \rho v \\ \rho u v - B_y B_x \\ \rho v^2 + p_t - B_y^2 \\ \rho w v - B_y B_z \\ B_x v - B_y u \\ \psi \\ B_z v - B_y w \\ (\rho e + p_t) v - B_y (\mathbf{V} \cdot \mathbf{B}) \\ c_h^2 B_y \end{bmatrix}, \quad H = \begin{bmatrix} 0 \\ 0 \\ 0 \\ 0 \\ 0 \\ 0 \\ 0 \\ 0 \\ -\frac{c_h^2}{c_p^2}\psi \end{bmatrix} \tag{3}$$

where ρ, p, $\mathbf{V}$, $\mathbf{B}$, e, and ψ are density, pressure, velocity field, magnetic field, specific total energy, and Lagrange multiplier, respectively. Total pressure and specific total energy are given by

$$p_t = p + \tfrac{1}{2}(B_x^2 + B_y^2 + B_z^2) \tag{4}$$

$$\rho e = \frac{p}{\gamma - 1} + \frac{1}{2}\rho(u^2 + v^2 + w^2) + \frac{1}{2}(B_x^2 + B_y^2 + B_z^2) \tag{5}$$

In the hyperbolic divergence cleaning method, c_h and c_p are the parameters that characterize the hyperbolic and parabolic properties. The c_h and c_p are given by

$$\Delta t = CFL \min_{(i,j)\in D} \min\left(\frac{\Delta x}{c_f^x}, \frac{\Delta y}{c_f^y}\right)_{i,j} \tag{6}$$

where

$$c_f^x = [\{\gamma p + |\vec{B}|^2 + \sqrt{(\gamma p + |\vec{B}|^2)^2 - 4\gamma p B_x^2}\}/2\rho]^{1/2}$$

$$c_f^y = [\{\gamma p + |\vec{B}|^2 + \sqrt{(\gamma p + |\vec{B}|^2)^2 - 4\gamma p B_y^2}\}/2\rho]^{1/2}$$

and D is a computational domain

$$c_h = \frac{CFL}{\Delta t} \min_{(i,j)\in D} \min(\Delta x, \Delta y)_{i,j} \tag{7a}$$

$$c_p(c_d, c_h, \Delta t) = \sqrt{-\Delta t \frac{c_h^2}{\ell_n(c_d)}}, \qquad \text{where } c_d \in (0,1) \tag{7b}$$

The detailed explanations of the hyperbolic divergence cleaning method are described in [37].

III. Numerical Method

In the present section, AUSMPW + /M-AUSMPW+ schemes [30,31] for gas dynamics are extended to the ideal MHD equations.

A. AUSMPW+ for Gas Dynamics

AUSMPW+ can be briefly written as follows:

$$\mathbf{F}_{\frac{1}{2}} = \bar{M}_L^+ c_{\frac{1}{2}} \mathbf{\Phi}_L + \bar{M}_R^- c_{\frac{1}{2}} \mathbf{\Phi}_R + (P_L^+ \mathbf{P}_L + P_R^- \mathbf{P}_R) \tag{8}$$

where $\mathbf{P} = (0, p, 0)^T$ and $\Phi = (\rho, \rho u, \rho H)^T$. The subscripts $\frac{1}{2}$ and (L, R) represent a cell-interface quantity and the left and right states across a cell interface, respectively.

$\bar{M}_{L,R}^{\pm}$ is the Mach number interpolation function

$$m_{\frac{1}{2}} = M_L^+ + M_R^- \geq 0,$$
$$\bar{M}_L^+ = M_L^+ + M_R^- \cdot [(1-w)\cdot(1+f_R) - f_L]$$
$$\bar{M}_R^- = M_R^- \cdot w \cdot (1+f_R) \tag{9a}$$

$$m_{\frac{1}{2}} < 0,$$
$$\bar{M}_L^+ = M_L^+ \cdot w \cdot (1+f_L)$$
$$\bar{M}_R^- = M_R^- + M_L^+ \cdot [(1-w)\cdot(1+f_L) - f_R)] \tag{9b}$$

where the functions f and w are pressure-based weight functions.

The AUSMPW+ has been developed to eliminate the oscillatory behaviors of AUSM-type schemes. AUSM-type schemes generally show good accuracy, robustness, and efficiency, which are necessary characteristics especially in hypersonic and reactive flow simulations. However, the advection characteristic of AUSM-type schemes should be treated carefully because it is the direct cause of numerical overshoots or oscillations. By controlling the advection characteristic with weight functions f and w, AUSMPW+ can successfully remove the overshoot phenomenon without compromising efficiency and accuracy. Details are in [30].

B. M-AUSMPW+ for Gas Dynamics

In M-AUSMPW+, the convective flux is modified from Eqs. (8–10) to reduce the numerical dissipation in a smooth region effectively:

$$\mathbf{F}_{\frac{1}{2}} = \bar{M}_L^+ c_{\frac{1}{2}} \mathbf{\Phi}_{L,\frac{1}{2}} + \bar{M}_R^- c_{\frac{1}{2}} \mathbf{\Phi}_{R,\frac{1}{2}} + (P_L^+ \mathbf{P_L} + R_R^- \mathbf{P_R}) \tag{10}$$

where $\mathbf{\Phi}_{L,R,\frac{1}{2}}$ is the modified convective quantity in a cell-interface.

The M-AUSMPW+ automatically distinguishes a smooth region from a rapidly varying region based on the criteria of Eqs. (11a) and (11b). The convective quantity is modified only in the smooth region to enhance the solution accuracy. In a rapidly varying region, the convective quantity is not modified because of stability problems. In M-AUSMPW+, Eq. (11a) is used as the definition of a rapidly varying region and Eq. (11b) is that of a smooth region:

$$\text{Rapidly varying region}: \bar{\mathbf{\Phi}}_i \leq \mathbf{\Phi}_R < \mathbf{\Phi}_L \leq \bar{\mathbf{\Phi}}_{i+1} \tag{11a}$$

$$\text{Smooth region}: \bar{\mathbf{\Phi}}_i \leq \mathbf{\Phi}_L < \mathbf{\Phi}_R \leq \bar{\mathbf{\Phi}}_{i+1} \tag{11b}$$

where $\bar{\mathbf{\Phi}}_i$ and $\bar{\mathbf{\Phi}}_{i+1}$ are the cell averaged values at each cell and $\mathbf{\Phi}_L$ and $\mathbf{\Phi}_R$ are the point values at the cell interface between cell i and $i+1$.

Finally, the convective quantity of the M-AUSMPW+ scheme at the cell-interface is formulated as follows:

$$\mathbf{\Phi}_{L,\frac{1}{2}} = \mathbf{\Phi}_L + \frac{\max[0, (\mathbf{\Phi}_R - \mathbf{\Phi}_L)(\mathbf{\Phi}_{L,\text{superbee}} - \mathbf{\Phi}_L)]}{(\mathbf{\Phi}_R - \mathbf{\Phi}_L)|\mathbf{\Phi}_{L,\text{superbee}} - \mathbf{\Phi}_L|} \times \min\left[a\frac{|\mathbf{\Phi}_R - \mathbf{\Phi}_L|}{2}, |\mathbf{\Phi}_{L,\text{superbee}} - \mathbf{\Phi}_L|\right] \tag{12a}$$

$$\mathbf{\Phi}_{R,\frac{1}{2}} = \mathbf{\Phi}_R + \frac{\max[0, (\mathbf{\Phi}_L - \mathbf{\Phi}_R)(\mathbf{\Phi}_{R,\text{superbee}} - \mathbf{\Phi}_R)]}{(\mathbf{\Phi}_L - \mathbf{\Phi}_R)|\mathbf{\Phi}_{R,\text{superbee}} - \mathbf{\Phi}_R|} \times \min\left[a\frac{|\mathbf{\Phi}_L - \mathbf{\Phi}_R|}{2}, |\mathbf{\Phi}_{R,\text{superbee}} - \mathbf{\Phi}_R|\right] \tag{12b}$$

where $a = 1 - \min(1, \max(|M_L|, |M_R|))^2$. Its derivative is continuous when the Mach number becomes zero. The details are presented in [31].

C. Modifications of AUSMPW + /M-AUSMPW+ Schemes for the Ideal MHD Equations

AUSM-type schemes used to analyze the ideal MHD equations have been investigated in several studies. Agarwal and Augustinus [29] applied the original AUSM scheme to the ideal MHD equations for Brio–Wu's one-dimensional shock-tube problem. Pan et al. [38] exploited the AUSM+ scheme to solve the Brio–Wu one-dimensional shock-tube problem and the problem of two-dimensional nozzle flows with a magnetic field. Their studies, however, were insufficient in proving the accuracy and robustness of the AUSM-type schemes because they just focused on the applicability of the AUSM-type scheme to ideal MHD flows, and the test problems that were solved were very simple cases. Also, the combination with high-order schemes was much more probable to yield numerical oscillations in a shock wave, which led to calculation failure. Therefore, in order to analyze the MHD equations accurately and robustly, the AUSM-type scheme had to be improved to raise its capability to handle oscillations without loss of accuracy. In the present study, we used the AUSMPW + /M-AUSMPW+ scheme as the base flux functions and modified them to overcome the weaknesses of the AUSM-type schemes. The key idea of the AUSMPW + /M-AUSMPW+ scheme is to remove the numerical oscillation by sensing the discontinuous region and controlling the advection characteristic with the pressure-based weight functions. To apply the key idea to the ideal MHD equations, pressure-based weight functions f and w were modified to consider a magnetic field.

1. Modification of Function f

To determine an appropriate model for the function f, the one-dimensional Ryu and Jones [9] shock-tube problem was calculated. The models f_1 and f_2 were tested and compared with each other. One was the original AUSMPW+ model, as in Eq. (13), which only considers the thermal pressure, and the other one was the modified model, which considers both thermal pressure and magnetic pressure, as in Eq. (14). For the pressure-based weight function w, the original form of the AUSMPW+ scheme was used, as in Eq. (15).

Model f_1, *Original* AUSMPW+:

$$f_{1,L,R} = \begin{cases} (\frac{p_L, p_R}{p_s} - 1), & p_s \neq 0 \\ 0, & \text{elsewhere} \end{cases}, \qquad p_s = P_L^+ p_L + P_R^- p_R \tag{13}$$

Model f_2, *Modified* AUSMPW+:

$$f_{2,L,R} = \begin{cases} (\frac{p_{t,L}, p_{t,R}}{p_{ts}} - 1), & p_{ts} \neq 0 \\ 0, & \text{elsewhere} \end{cases}, \qquad p_{ts} = P_L^+ p_{t,L} + P_R^- p_{t,R} \tag{14}$$

where

$$p_{t,L} = p_L + \tfrac{1}{2}(B_x^2 + B_y^2 + B_z^2)_L$$

$$p_{t,R} = p_R + \tfrac{1}{2}(B_x^2 + B_y^2 + B_z^2)_R$$

$$w(p_L, p_R) = 1 - \min\left(\frac{p_L}{p_R}, \frac{p_R}{p_L}\right)^3 \tag{15}$$

The initial states of the left and right cells of Ryu and Jones' MHD shock tube were given by

$$(\rho, u, v, w, B_y, B_z, p)_L = [1.08, 1.2, 0.01, 0.5, 3.6/(4\pi)^{1/2}, 3.6/(4\pi)^{1/2}, 0.95] \tag{16a}$$

$$(\rho, u, v, w, B_y, B_z, p)_R = [1, 0, 0, 0, 4/(4\pi)^{1/2}, 2/(4\pi)^{1/2}, 1] \tag{16b}$$

with $B_x = 2/(4\pi)^{1/2}$ and $\gamma = 5/3$.

The CFL number was 0.8, and 800 grid points were used for numerical calculations. The calculated results were compared and analyzed at time $t = 0.08$ s. For this test, the second-order MUSCL-TVD (monotone upstream-centered scheme for conservation laws-total variation diminishing) with the van Leer limiter was applied and the third-order TVD Runge–Kutta method was used for time integration.

Figures 1 and 2 show the density plots obtained from both models f_1 and f_2. In Fig. 2, the magnified rectangular region of Fig. 1, model f_1 shows oscillatory behaviors whereas model f_2 eliminates them effectively by accounting for the effect of the magnetic field in the function f. Throughout this test, it was confirmed that the consideration of the magnetic field influenced the discontinuity capturing ability of AUSMPW+ and that model f_2 was an appropriate choice as the pressure-based weight function f for the ideal MHD equations.

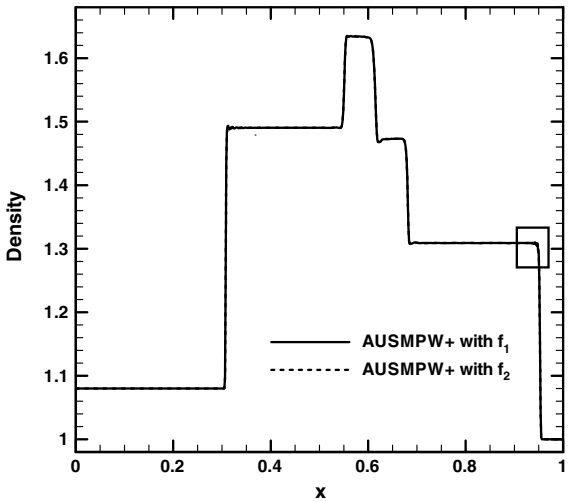

Fig. 1 Solution of density plot of Ryu and Jones' shock-tube problem. The solid line is the solution of the original AUSMPW+ using function model f_1 and the dashed line is the solution using the modified function model f_2.

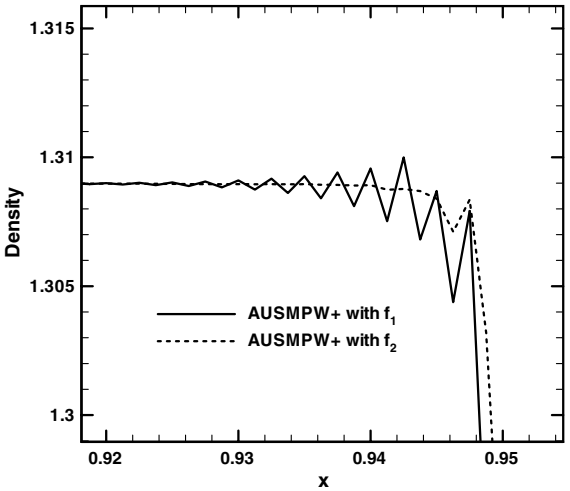

Fig. 2 Comparison of density distribution at the rectangular region in Fig. 1.

2. Modification of Function w

The other pressure-based weight function w was determined by procedures similar to those of function f. One was the original model used in the original AUSMPW+ scheme, which only considered the thermal pressure, as in Eq. (17), and the other one was the modified model, which used the total pressure (thermal pressure + magnetic pressure) to consider the effect of the magnetic field, as shown in Eq. (18). As for the function f, the modified model f_2 of Eq. (14) was used:

Model w_1, *Original* AUSMPW+:

$$w_1(p_L, p_R) = 1 - \min\left(\frac{p_L}{p_R}, \frac{p_R}{p_L}\right)^3 \tag{17}$$

Model w_2, *Modified* AUSMPW+:

$$w_2(p_{t,L}, p_{t,R}) = 1 - \min\left(\frac{p_{t,L}}{p_{t,R}}, \frac{p_{t,R}}{p_{t,L}}\right)^3 \tag{18}$$

where

$$p_{t,L} = p_L + \tfrac{1}{2}(B_x^2 + B_y^2 + B_z^2)_L$$

$$p_{t,R} = p_R + \tfrac{1}{2}(B_x^2 + B_y^2 + B_z^2)_R$$

Among the one-dimensional Ryu and Jones MHD shock-tube problems in [9], the following test case was chosen for determining the function w. The initial conditions of the left and right cells for the test were given by

$$(\rho, u, v, w, B_y, B_z, p)_L = [1, 0, 0, 0, 1, 0, 1] \tag{19a}$$

$$(\rho, u, v, w, B_y, B_z, p)_R = [0.2, 0, 0, 0, 0, 0, 0.1] \tag{19b}$$

with $B_x = 1$, $\gamma = 5/3$.

The CFL number was 0.8, and 800 grid points were used. For this test, the second-order MUSCL-TVD with the van Leer limiter was applied, and the third-order TVD Runge—Kutta method was used for time integration. Figure 3 shows spatial distributions of the density for the models w_1 and w_2. To investigate the numerical

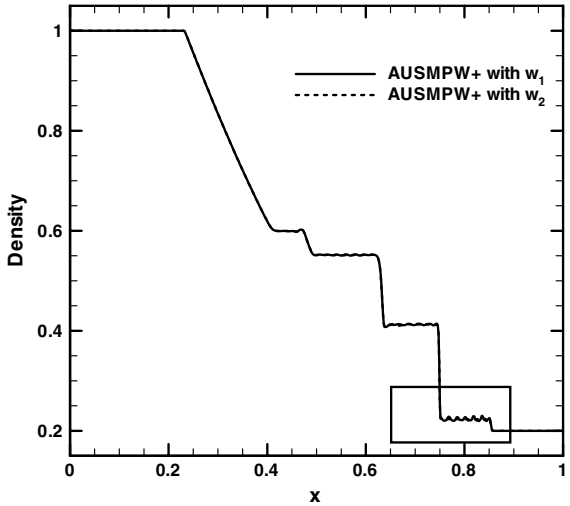

Fig. 3 Density distribution of Ryu and Jones' shock-tube problem according to models w_1 and w_2.

characteristics of the models precisely, the rectangular region in Fig. 3 was enlarged. As shown in Fig. 4, the modified model w_2 can eliminate the numerical oscillations dramatically whereas the original model w_1 shows higher oscillations. In Ryu and Jones' MHD shock-tube problems, it was proven that the modified functions f_2 and w_2 could remove the numerical oscillations effectively by taking the magnetic field into account.

3. *Advantage of f_2 and w_2 in Capturing Stationary Contact Discontinuity*

The modified pressure-based weight functions, f_2 and w_2, have the advantage in capturing a stationary contact discontinuity of MHD equations. Generally, a contact discontinuity is characterized by a zero normal velocity $V_n = 0$ and a nonzero density jump $\rho_L \neq \rho_R$ across the discontinuity. The MHD equations have these two kinds of contact discontinuities [39]. When the normal magnetic field is not zero $B_n \neq 0$ the jump conditions' characteristics are as follows: the constant tangential velocity, magnetic field and pressure, $\mathbf{V}_{t,L} = \mathbf{V}_{t,R}$, $\mathbf{B}_L = \mathbf{B}_R$, and $p_L = p_R$, that is, the density only changes across the discontinuity, and this is commonly called a contact discontinuity. The other type occurs when $B_n = 0$ and it has the following jump conditions: $\mathbf{V}_{t,L} \neq \mathbf{V}_{t,R}$, $\mathbf{B}_{t,L} \neq \mathbf{B}_{t,R}$, and constant total pressure, $p_L + \mathbf{B}_L^2/2 = p_R + \mathbf{B}_R^2/2$. This type of contact discontinuity is called a tangential discontinuity.

To capture the discontinuities exactly, the numerical fluxes must be equal to the following exact fluxes for stationary contact and tangential discontinuities across a cell interface in Fig. 5.

1) *Contact discontinuity*:

$$\text{mass flux}: F_{1,\text{exact}} = 0 \tag{20a}$$

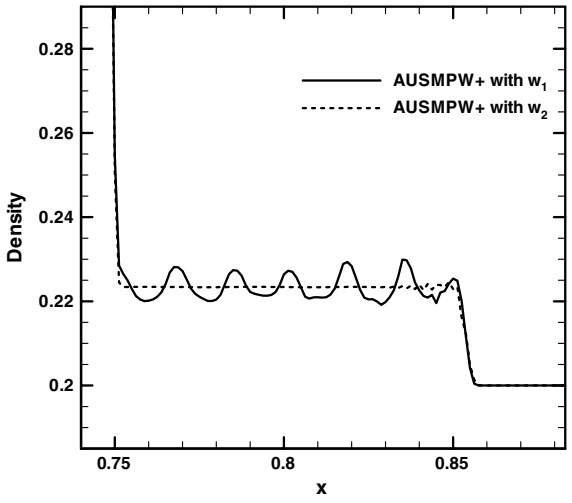

Fig. 4 Comparison of density distribution at the rectangular region in Fig. 3.

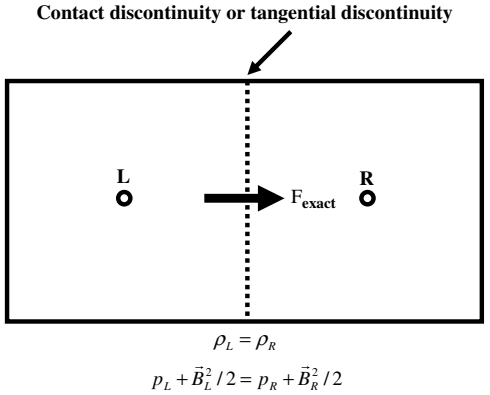

Fig. 5 Flow conditions for stationary contact or tangential discontinuity.

$$\begin{gathered}\text{momentum flux}: F_{2,x,\text{exact}} = p_{t,L} - B_{x,L}^2 \\ F_{2,y,\text{exact}} = -B_{y,L}B_{x,L}, \qquad F_{2,z,\text{exact}} = -B_{z,L}B_{x,L}\end{gathered} \tag{20b}$$

$$\begin{gathered}\text{magnetic flux}: F_{3,x,\text{exact}} = 0, \qquad F_{3,y,\text{exact}} = -B_{x,L}v_L \\ F_{3,z,\text{exact}} = -B_{x,L}w_L\end{gathered} \tag{20c}$$

$$\text{energy flux}: F_{4,\text{exact}} = -B_{x,L}(v_L B_{y,L} + w_L B_{z,L}) \tag{20d}$$

2) *Tangential discontinuity*:

$$\text{mass flux}: F_{1,\text{exact}} = 0 \tag{21a}$$

$$\begin{gathered}\text{momentum flux}: F_{2,x,\text{exact}} = p_{t,L}, \qquad F_{2,y,\text{exact}} = 0 \\ F_{2,z,\text{exact}} = 0\end{gathered} \tag{21b}$$

$$\text{magnetic flux}: F_{3,x,\text{exact}} = 0, \qquad F_{3,y,\text{exact}} = 0, \qquad F_{3,z,\text{exact}} = 0 \tag{21c}$$

$$\text{energy flux}: F_{4,\text{exact}} = 0 \tag{21d}$$

3) The numerical *mass flux* of AUSMPW+ using the modified pressure-based weight functions f_2 and w_2 for contact and tangential discontinuities can be written by

$$\begin{aligned}F_1 = \bar{M}_L^+ c_{\frac{1}{2}}\rho_L + \bar{M}_R^- c_{\frac{1}{2}}\rho_R = \{&\tfrac{1}{4}\cdot w_2\cdot(1+f_{2,R}) \\ &-\tfrac{1}{4}(f_{2,R}-f_{2,L})\}c_{\frac{1}{2}}\rho_L + \{-\tfrac{1}{4}\cdot w_2\cdot(1+f_{2,R})\}c_{\frac{1}{2}}\rho_R = F_{1,\text{exact}} = 0\end{aligned} \tag{22}$$

For the exact mass flux, that is, $F_1 = F_{1,\text{exact}} = 0$ w_2 has to be zero and $f_{2,L}$ has to be equal to $f_{2,R}$. Because the total pressure (thermal pressure + magnetic pressure) is conserved across the both contact and tangential discontinuities,

$$w_2 = 1 - \min(p_{t,L}/p_{t,R}, p_{t,R}/p_{t,L})^3$$

automatically becomes zero and $f_{2,L} = f_{2,R} = 0$. Thus, numerical mass flux F_1 of modified AUSMPW+ equals the exact mass flux in Eq. (20a) and (21a).

4) *Momentum flux*:

$$\begin{aligned}F_{2,x} = \bar{M}_L^+ c_{\frac{1}{2}}(\rho u)_L + \bar{M}_R^- c_{\frac{1}{2}}(\rho u)_R + (P_L^+ p_{t,L} + P_R^- p_{t,R}) \\ -\frac{B_{x,L}^2 + B_{x,R}^2}{2} = p_{t,L} - \frac{B_{x,L}^2 + B_{x,R}^2}{2}\end{aligned} \tag{23a}$$

$$\text{contact discontinuity}: F_{2,x} = p_{t,L} - B_{x,L}^2 = F_{2,x,\text{exact}} \tag{23b}$$

$$\text{tangential discontinuity}: F_{2,x} = p_{t,L} = F_{2,x,\text{exact}} \tag{23c}$$

$$\begin{aligned}F_{2,y} = \bar{M}_L^+ c_{\frac{1}{2}}(\rho v)_L + \bar{M}_R^- c_{\frac{1}{2}}(\rho v)_R + (P_L^+\cdot 0 + P_R^-\cdot 0) \\ -\frac{(B_{y,L}B_{x,L} + B_{y,R}B_{x,R})}{2} = -\frac{(B_{y,L}B_{x,L} + B_{y,R}B_{x,R})}{2}\end{aligned} \tag{24a}$$

$$\text{contact discontinuity}: F_{2,y} = -B_{y,L}B_{x,L} = F_{2,y,\text{exact}} \tag{24b}$$

$$\text{tangential discontinuity}: F_{2,y} = 0 = F_{2,y,\text{exact}} \tag{24c}$$

$$F_{2,z} = \bar{M}_L^+ c_{\frac{1}{2}}(\rho w)_L + \bar{M}_R^- c_{\frac{1}{2}}(\rho w)_R + (P_L^+ \cdot 0 + P_R^- \cdot 0) - \frac{(B_{z,L}B_{x,L} + B_{z,R}B_{x,R})}{2} = -\frac{(B_{z,L}B_{x,L} + B_{z,R}B_{x,R})}{2} \quad (25a)$$

$$\text{contact discontinuity}: F_{2,z} = -B_{z,L:}B_{x,L} = F_{2,z,\text{exact}} \quad (25b)$$

$$\text{tangential discontinuity}: F_{2,z} = 0 = F_{2,z,\text{exact}} \quad (25c)$$

5) *Magnetic flux*:

$$F_{3,x} = \bar{M}_L^+ c_{\frac{1}{2}}B_{x,L} + \bar{M}_R^- c_{\frac{1}{2}}B_{x,R} + (P_L^+(-B_{x,L}u_L) + P_R^-(-B_{x,R}u_R)) = 0 \quad (26a)$$

$$\text{contact discontinuity}: F_{3,x} = 0 = F_{3,x,\text{exact}} \quad (26b)$$

$$\text{tangential discontinuity}: F_{3,x} = 0 = F_{3,x,\text{exact}} \quad (26c)$$

$$F_{3,y} = \bar{M}_L^+ c_{\frac{1}{2}}B_{y,L} + \bar{M}_R^- c_{\frac{1}{2}}B_{y,R} + (P_L^+(-B_{x,L}v_L) + P_R^-(-B_{x,R}v_R)) = \frac{-B_{x,L}v_L - B_{x,R}v_R}{2} \quad (27a)$$

$$\text{contact discontinuity}: F_{3,y} = -B_{x,L}v_L = F_{3,y,\text{exact}} \quad (27b)$$

$$\text{tangential discontinuity}: F_{3,y} = 0 = F_{3,y,\text{exact}} \quad (27c)$$

$$F_{3,y} = \bar{M}_L^+ c_{\frac{1}{2}}B_{z,L} + \bar{M}_R^- c_{\frac{1}{2}}B_{z,R} + (P_L^+(-B_{x,L}w_L) + P_R^-(-B_{x,R}w_R)) = \frac{-B_{x,L}w_L - B_{x,R}w_R}{2} \quad (28a)$$

$$\text{contact discontinuity}: F_{3,z} = -B_{x,L}w_L = F_{3,z,\text{exact}} \quad (28b)$$

$$\text{tangential discontinuity}: F_{3,z} = 0 = F_{3,z,\text{exact}} \quad (28c)$$

6) *Energy flux*:

$$F_4 = \bar{M}_L^+ c_{\frac{1}{2}}(\rho e + p_t)_L + \bar{M}_R^- c_{\frac{1}{2}}(\rho e + p_t)_R + P_L^+(-B_{x,L}(\mathbf{V}\cdot\mathbf{B})_L) + P_R^+(-B_{x,R}(\mathbf{V}\cdot\mathbf{B})_R) = \frac{-B_{x,L}(\mathbf{V}\cdot\mathbf{B})_L - B_{x,R}(\mathbf{V}\cdot\mathbf{B})_R}{2} \quad (29a)$$

$$\text{contact discontinuity}: F_4 = -B_{x,L}(v_L B_{y,L} + w_L B_{z,L}) = F_{4,z,\text{exact}} \quad (29b)$$

$$\text{tangential discontinuity}: F_{4,z} = 0 = F_{4,\text{exact}} \quad (29c)$$

Because all numerical fluxes across contact discontinuities are exactly the same as the physical fluxes, the modified AUSMPW+ can capture stationary contact and tangential discontinuities perfectly. The modified ASUMPW+ using f_2 and w_2 functions was tested for the following conditions of stationary contact and tangential discontinuities.

Contact discontinuity:

$$(\rho, u, v, w, B_x, B_y, B_z, p)_L = [1, 0, 0, 0, 1, 0, 0, 1]$$
$$(\rho, u, v, w, B_x, B_y, B_z, p)_R = [10, 0, 0, 0, 1, 0, 0, 1] \quad (30)$$

Tangential discontinuity:

$$(\rho, u, v, w, B_x, B_y, B_z, p)_L = [1, 0, 5, 5, 0, 2, 1, 2.5]$$
$$(\rho, u, v, w, B_x, B_y, B_z, p)_R = [10, 0, 1, 1, 0, \sqrt{5}, \sqrt{3}, 2] \quad (31)$$

The results show that AUSMPW+ using the modified pressure-based weight functions can calculate a stationary contact and a tangential discontinuity exactly and do not have any dissipation, whereas the original AUSMPW+ generates numerical dissipation for the tangential discontinuity, as shown in Fig. 6.

Conclusively, the modified pressure-based weight functions f_2 and w_2 defined in terms of the total pressure can handle numerical oscillations at a strong shock wave, and they can resolve stationary contact and tangential discontinuities without any dissipation.

4. *Accuracy Improvement by* M-AUSMPW+ *Scheme*

The newly modified AUSMPW+ scheme for the ideal MHD was compared with a Roe-type linearized Riemann solver to investigate its accuracy, especially with respect to a moving contact discontinuity. The Ryu and Jones MHD shock-tube problem, which was the test problem for determining the function f, was calculated again. The CFL number was 0.8, 2000 grid points were used, and all other conditions were the same as those of the previous calculations.

Figure 7 shows spatial distributions of density calculated by the modified AUSMPW+ scheme and Roe-type linearized Riemann solvers, which were constructed by referring to [8,34]. As seen in Fig. 8, the magnified elliptic region of Fig. 7, the Roe-type solver produces a severe oscillatory phenomenon behind the strong shock wave whereas the modified AUSMPW+ scheme restricts the oscillations effectively by using the modified pressure-based weight functions. However, in Fig. 9a, which is the enlarged profile of moving contact discontinuity, the modified AUSMPW+ scheme captures it more diffusively than Roe-type linearized Riemann solvers, that is, the modified AUSMPW+ has more numerical dissipation at the moving contact wave. Thus, in order to enhance the accuracy at a moving contact discontinuity, the M-AUSMPW+ scheme, which was designed to minimize numerical dissipation, is

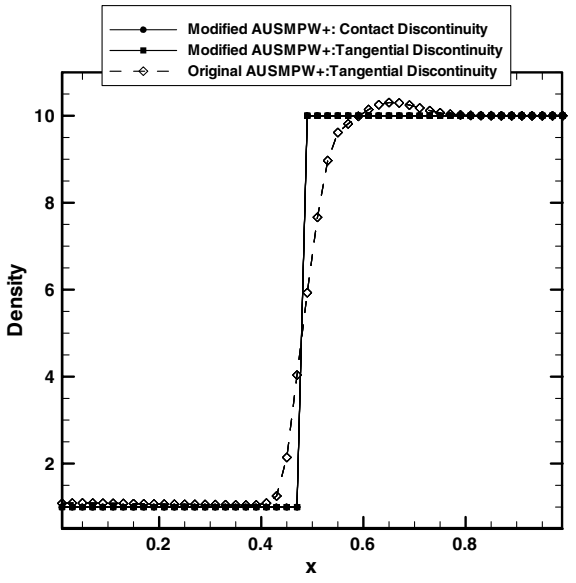

Fig. 6 Density distribution of stationary contact and tangential discontinuities.

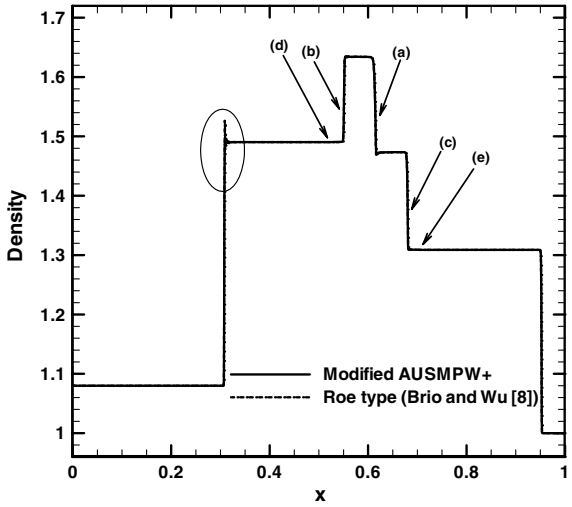

Fig. 7 Density distribution according to the numerical flux functions for Roe-type and modified AUSMPW+ schemes.

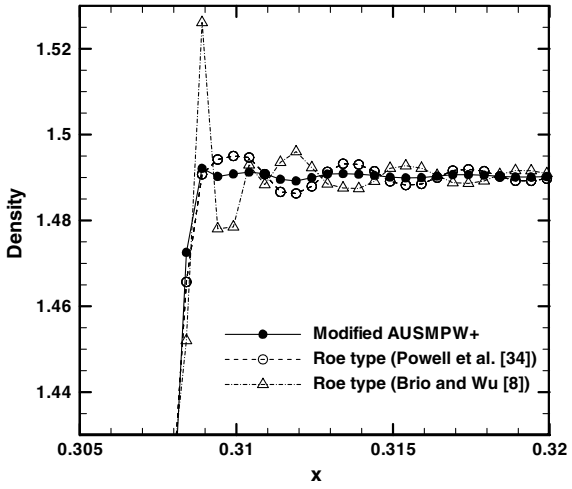

Fig. 8 Comparison of density plot between Roe-type and modified AUSMPW+ at the elliptic region in Fig. 7.

introduced here. The convective quantity at a cell interface for MHD equations is shown in Eqs. (12a) and (12b) where

$$a = 1 - \min(1, \max(|M_L|, |M_R|))^2$$

The speed of a fast magnetosonic wave is used to define the Mach number, that is, $M = \frac{u}{c_f}$.

As seen in Fig. 9, the results computed by the modified M-AUSMPW+ show a more enhanced accuracy in all MHD waves, including rotational discontinuities and slow shock waves, than those by the modified AUSMPW+ and even those by the Roe-type solver. It is interesting that in Figs. 9c and 9e, which represent the right slow shock wave and right rotational discontinuities, respectively, the modified AUSMPW+ is seen to be more accurate than the Roe-type solver whereas the opposite results are observed from Figs. 9b and 9d.

D. Extension of Modified AUSMPW + /M-AUSMPW+ Schemes to Two-Dimensional MHD Equations

The modified numerical flux of AUSMPW + /M-AUSMPW+ in two dimensions can be summarized as follows:

$$\mathbf{\Phi} = \begin{bmatrix} \rho \\ \rho u \\ \rho v \\ \rho w \\ B_x \\ B_y \\ B_z \\ (\rho e + p_t) \\ 0 \end{bmatrix}, \qquad \mathbf{P} = \begin{bmatrix} 0 \\ \xi_x p_t \\ \xi_y p_t \\ 0 \\ -\bar{B}_{n,\frac{1}{2}} u \\ -\bar{B}_{n,\frac{1}{2}} v \\ -\bar{B}_{n,\frac{1}{2}} w \\ -\bar{B}_{n,\frac{1}{2}} (\mathbf{V}\cdot\mathbf{B}) \\ 0 \end{bmatrix}$$

$$\mathbf{F}_B = \begin{bmatrix} 0 \\ -B_x \bar{B}_{n,\frac{1}{2}} \\ -B_y \bar{B}_{n,\frac{1}{2}} \\ -B_z \bar{B}_{n,\frac{1}{2}} \\ \xi_x \psi \\ \xi_y \psi \\ 0 \\ 0 \\ c_h^2 \bar{B}_n \end{bmatrix} \tag{32}$$

where $\bar{B}_n = \xi_x B_x + \xi_y B_y$ and $\bar{B}_{n,\frac{1}{2}} = \frac{1}{2}(\bar{B}_{n,L} + \bar{B}_{n,R})$.

$$\mathbf{F}_{\frac{1}{2}} = \bar{M}_L^+ c_{\frac{1}{2}} \mathbf{\Phi}_{L,\frac{1}{2}} + \bar{M}_R^- c_{\frac{1}{2}} \mathbf{\Phi}_{R,\frac{1}{2}} + (P_L^+ \mathbf{P_L} + P_R^- \mathbf{P_R}) + \tfrac{1}{2}(\mathbf{F}_{B,L} + \mathbf{F}_{B,R}) \tag{33}$$

where

$$m_{\frac{1}{2}} = M_L^+ + M_R^- \geq 0$$
$$\bar{M}_L^+ = M_L^+ + M_R^- \cdot [(1-w)\cdot(1+f_R) - f_L]$$
$$\bar{M}_R^- = M_R^- \cdot w \cdot (1+f_R)$$

and

$$m_{\frac{1}{2}} < 0, \qquad \bar{M}_L^+ = M_L^+ \cdot w \cdot (1+f_L)$$
$$\bar{M}_R^- = M_R^- + M_L^+ \cdot [(1-w)\cdot(1+f_L) - f_R)]$$

l) A modified pressure-based weight functions f and w are shown

$$f_{2,L,R} = \begin{cases} (\frac{p_{t,L}-p_{t,R}}{p_{ts}} - 1), & p_{ts} \neq 0 \\ 0, & \text{elsewhere} \end{cases}, \qquad p_{ts} = P_L^+ p_{t,L} + P_R^- p_{t,R}$$

$$w_2(p_{t,L}, p_{t,R}) = 1 - \min\left(\frac{p_{t,L}}{p_{t,R}}, \frac{p_{t,R}}{p_{t,L}}\right)^3 \tag{18}$$

where

$$p_{t,L} = p_L + \tfrac{1}{2}(B_x^2 + B_y^2 + B_z^2)_L$$

and

$$p_{t,R} = p_R + \tfrac{1}{2}(B_x^2 + B_y^2 + B_z^2)_R$$

2) A modified AUSMPW+ scheme is shown as

$$\mathbf{\Phi}_{L,\frac{1}{2}} = \mathbf{\Phi}_L, \qquad \mathbf{\Phi}_{R,\frac{1}{2}} = \mathbf{\Phi}_R \tag{34}$$

3) A modified M-AUSMPW+ scheme is shown as

$$\mathbf{\Phi}_{L,\frac{1}{2}} = \mathbf{\Phi}_L + \frac{\max[0, (\mathbf{\Phi}_R - \mathbf{\Phi}_L)(\mathbf{\Phi}_{L,\text{superbee}} - \mathbf{\Phi}_L)]}{(\mathbf{\Phi}_R - \mathbf{\Phi}_L)|\mathbf{\Phi}_{L,\text{superbee}} - \mathbf{\Phi}_L|} \times \min\left[a\frac{|\mathbf{\Phi}_R - \mathbf{\Phi}_L|}{2}, |\mathbf{\Phi}_{L,\text{superbee}} - \mathbf{\Phi}_L|\right]$$

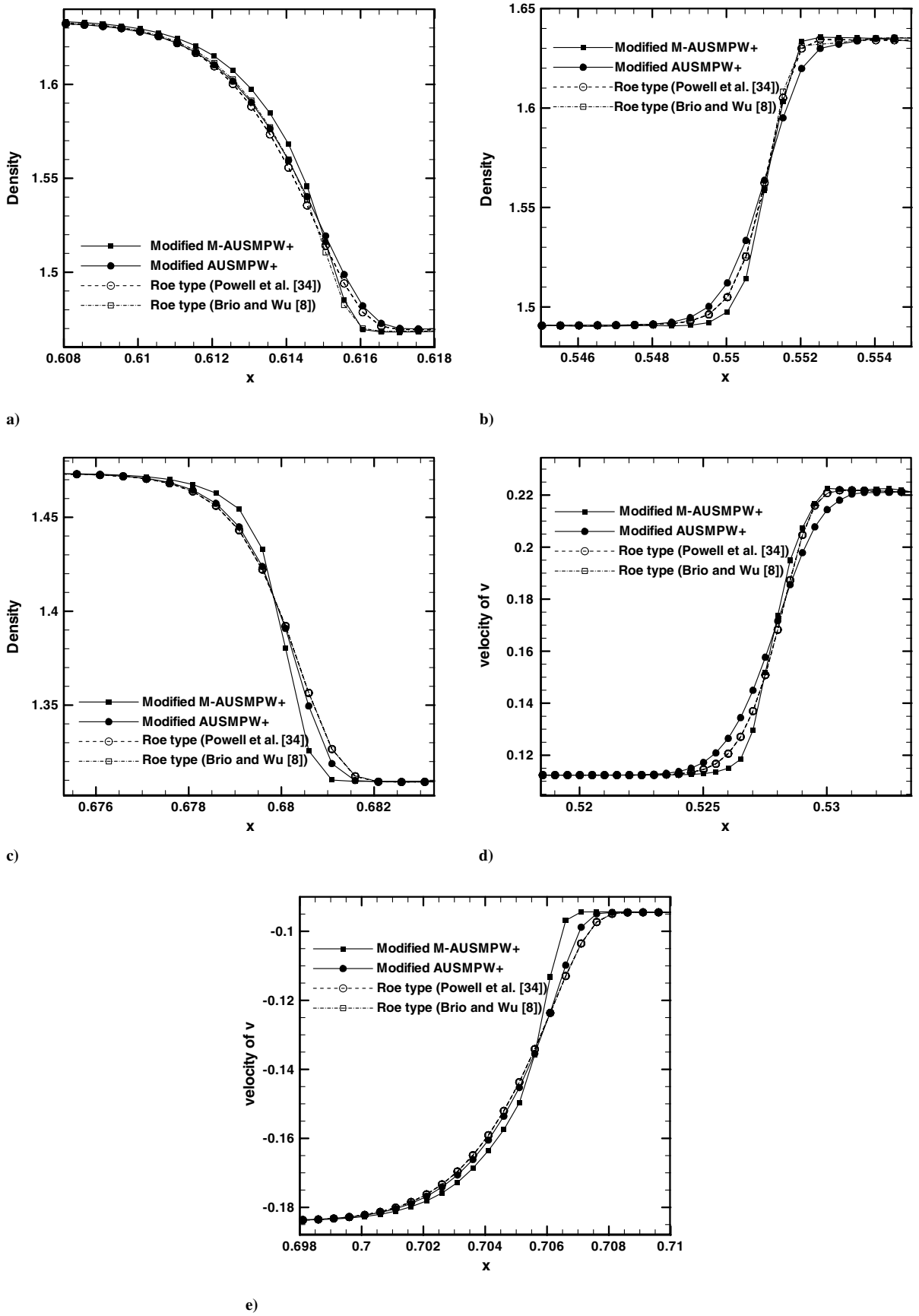

Fig. 9 Comparison of MHD waves at a) contact discontinuity, b) left slow shock wave, c) right slow shock wave, d) left rotational discontinuity, and e) right rotational discontinuity according to the numerical flux functions.

$$\Phi_{R,\frac{1}{2}} = \Phi_R + \frac{\max[0,(\Phi_L - \Phi_R)(\Phi_{R,\text{superbee}} - \Phi_R)]}{(\Phi_L - \Phi_R)|\Phi_{R,\text{superbee}} - \Phi_R|} \times \min\left[a\frac{|\Phi_L - \Phi_R|}{2}, |\Phi_{R,\text{superbee}} - \Phi_R|\right]$$

where

$$a = 1 - \min\left(1, \max\left(\left|\frac{u_L}{c_{f,L}}\right|, \left|\frac{u_R}{c_{f,R}}\right|\right)\right)^2$$

IV. Numerical Results

In this section, the modified AUSMPW + /M-AUSMPW+ schemes for the ideal MHD equations are verified by application to the two-dimensional Orszag–Tang MHD vortex problem. The modified AUSMPW + /M-AUSMWP+ schemes are compared with the Roe-type linearized Riemann solver with respect to accuracy, robustness, and efficiency.

For a two-dimensional numerical test, we chose the Orszag–Tang MHD vortex problem. Because it includes interactions of several shocks generated from the MHD equations and shows the crucial characteristics of an MHD vortex well, it is considered as one of the standard cases used to validate two-dimensional MHD codes [40,41].

The initial conditions are given by

$$\rho(x,y,0) = \gamma^2, \qquad u(x,y,0) = -\sin y, \qquad v(x,y,0) = \sin x \tag{35a}$$

$$p(x,y,0) = \gamma, \qquad B_x(x,y,0) = -\sin y, \qquad B_y(x,y,0) = \sin 2x \tag{35b}$$

where γ is 5/3.

The root-mean-square values of initial velocity and magnetic field are one, and the average Mach number is one. Double-periodic boundary conditions are given for both x and y directions.

All the CFL numbers used for the calculations are 0.8, and c_d in Eq. (7b) is 0.9. The computational domain is $[0, 2\pi] \times [0, 2\pi]$ with a uniform grid system. MUSCL–TVD with the van Leer limiter was used for the spatial interpolation, and the third-order TVD Runge–Kutta method was used for time integration. For the grid refinement study, our code was parallelized using the message passing interface (MPI) library.

The grid refinement tests were performed on 200×200, 400×400, 600×600, 800×800, 1000×1000, 1200×1200, 1400×1400, and 1600×1600 grid systems for the modified AUSMPW+, modified M-AUSMPW+, and Roe-type linearized Riemann solver, respectively. Pressure contours computed on the 200×200, 400×400, 800×800, and 1600×1600 grid systems using the modified AUSMPW+ are shown in Fig. 10 at time $t = 3$, respectively. Figure 11 shows the pressure lines plotted along the line AB in Fig. 10. As shown in Fig. 11, the results computed over the 400×400 grid size reached the grid convergence solution except for circular regions. Because these regions had a complex flow pattern, it was difficult to obtain the grid convergence solution even with the 1600×1600 grid size. It is expected from Fig. 12 that the grid convergence solution may be obtained on more than a 2000×2000 grid system in the region A. In the present paper, due to the memory limitation of our parallel machine, the results computed on the 1600×1600 grid system by using the modified AUSMPW+ scheme with the van Leer limiter was determined as the reference solution of the Orszag–Tang vortex problem.

To compare the accuracy of the developed schemes with that of the Roe-type linearized Riemann solver, the results from the schemes and the solver were compared with the reference solution. The computations of the Roe-type linearized Riemann solver using the van Leer limiter were run successfully on the grid systems from 200×200 to 1000×1000 without entropy fix. However, the Roe-type solver failed to provide a solution over the 1200×1200 grid system because of numerical oscillations. On the other hand, modified AUSMPW+ and M-AUSMPW+ were smoothly run up to the 1600×1600 grid system even with the van Leer limiter. As shown in Fig. 13, the result of the modified M-AUSMPW+ on the 800×800 grid system is closer to the reference solution than that of the Roe-type solver and that of the modified AUSMPW+ with the same grid size. In addition, the results of modified M-AUSMPW+ computed on the 1400×1400 and the 1200×1200 grid system are almost the same as those of modified AUSMPW+ on the 1600×1600 (reference solution) and the 1400×1400 grid system, respectively. It seems that the modified M-AUSMPW+ had the least amount of numerical dissipation among the other schemes and it can resolve the complex flows more accurately with a coarser grid system.

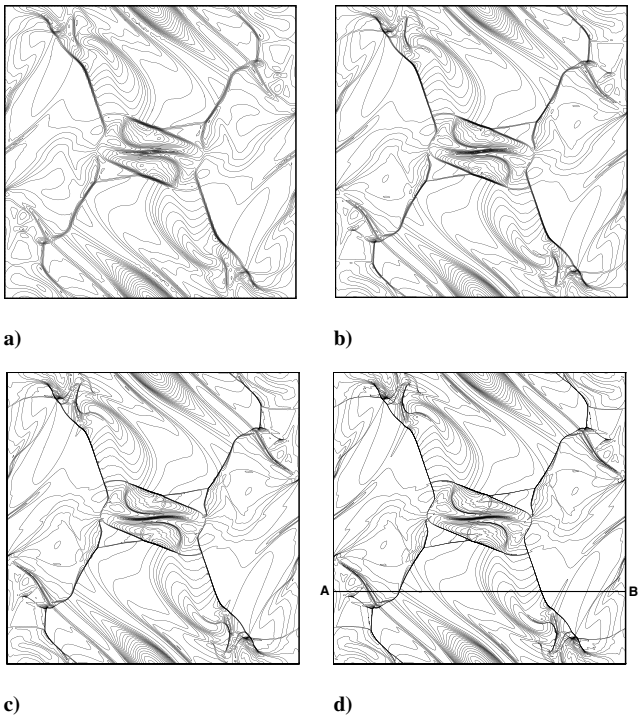

Fig. 10 Pressure contours by the modified AUSMPW+ at time $t = 3$. Shown are the results solved on a) 200 × 200, b) 400 × 400, c) 800 × 800, and d) 1600 × 1600 grid systems.

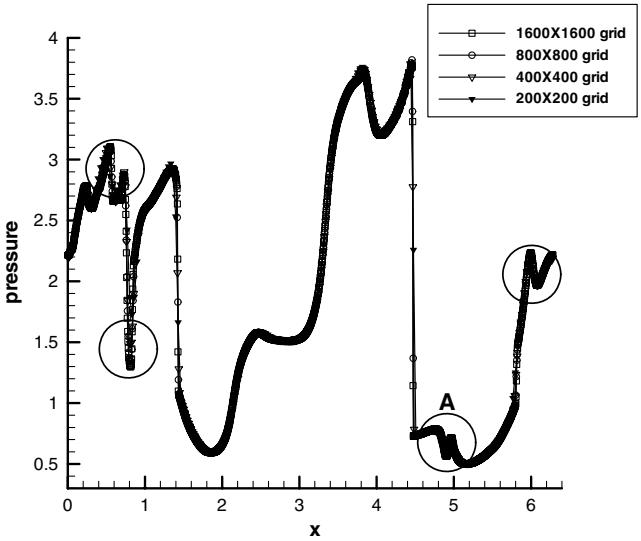

Fig. 11 Pressure line contour results of modified AUSMPW+ along the line AB in Fig. 10d.

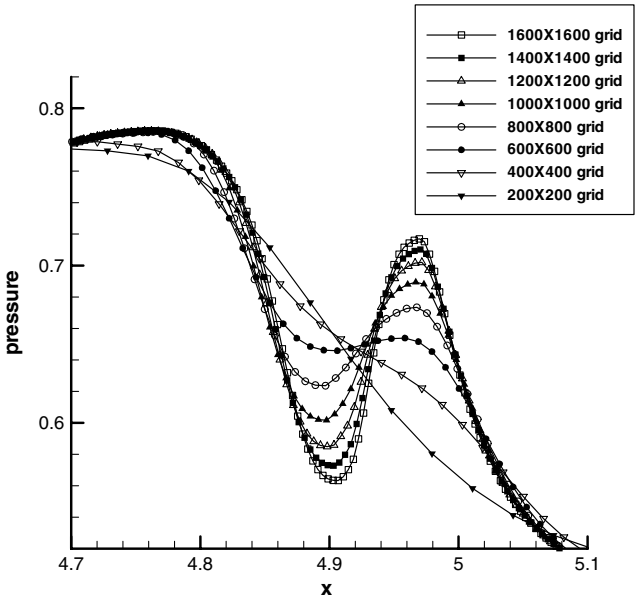

Fig. 12 Pressure line contours of the magnified region A of Fig. 11.

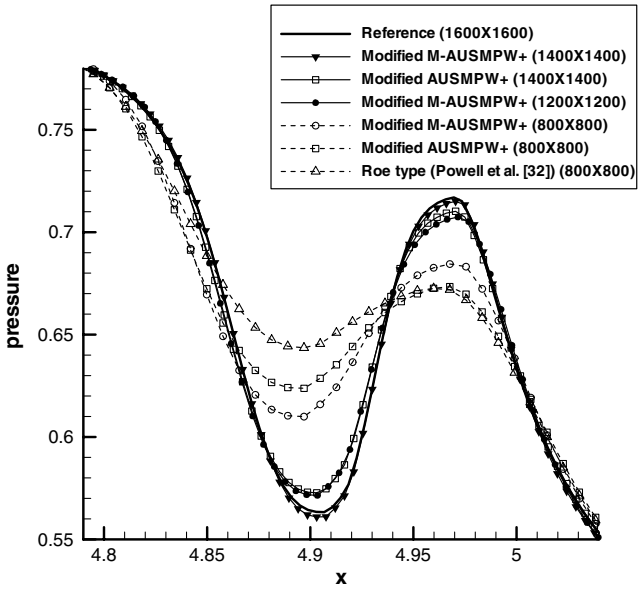

Fig. 13 Comparison of pressure line contours of the magnified region A of Fig. 11 for each scheme.

Concerning robustness, it was confirmed again through this test that the modified pressure-based weight functions were effective for improving robustness because they removed oscillations significantly. The original AUSMPW+ scheme could not perform the calculations stably even with the min-mod limiter because the original pressure-based weight functions could not take a magnetic field into account. Thus, it could not keep $\nabla \cdot \vec{B}$ as small values, and it ultimately amplified the divergence errors, as in Fig. 14. As shown in Fig. 15a, severe numerical oscillations of B_y are observed at the center of top and bottom sides, and in these regions all the primitive variables also oscillated. Because of the nonphysical oscillations, the computations by the original AUSMPW+ resulted in a blowup. On the other hand, because the modified pressure-based weight functions showed good ability for removing the oscillations, they provided nonoscillatory solutions, as shown in Fig. 15b.

Finally, we compared the computational efficiency of each scheme, and the results are tabulated in Table 1. The computations were mainly run on the parallel machine with 16 processors (2.0 GHz and 1 GB RAM per processor). As shown in Table 1, the modified AUSMPW+ had the superior efficiency. On the other hand, the Roe-type linearized Riemann solver took over one and a half times the computational time of the modified AUSMPW+. The results of Roe-type solver in Table 1 may change slightly according to how to construct the numerical dissipation term. However, it is not easy to reduce the computational time because linearized Riemann solvers basically have the eigen-decomposition process in the construction of numerical dissipation. In addition, linearized Riemann solvers will require explicitly more computational time for three-dimensional problems.

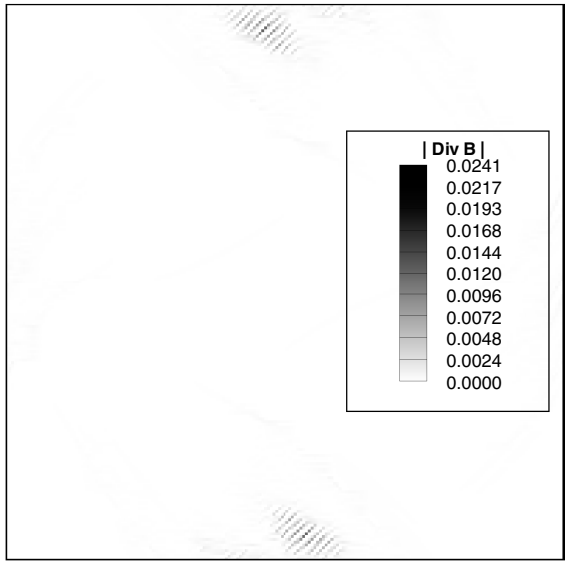

Fig. 14 Magnetic field divergence (Div B) contour of original AUSMPW+ scheme. Spurious divergence errors are produced and oscillated at the top and bottom sides.

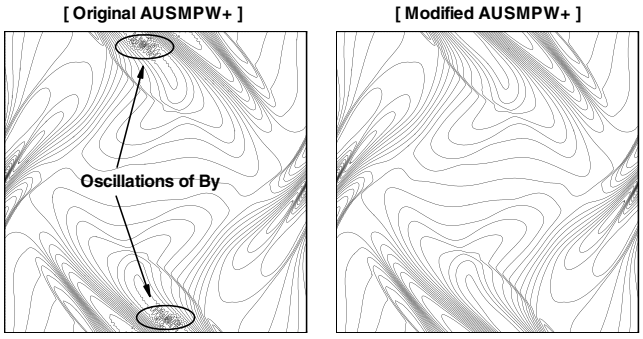

Fig. 15 Comparison of magnetic field *By* between the a) original AUSMPW+ and b) modified AUSMPW+ scheme at time $t = 1.4$. Original AUSMPW+ produces severe oscillations at the center of the top and bottom sides.

Table 1 Required time for calculation of Orszag and Tang's [40] vortex problem

Scheme	AUSMPW+	M-AUSMPW+	Roe-type FDS
400×400	1	1.21	1.52
600×600	1	1.25	1.54
800×800	1	1.23	1.52
1600×1600	1	1.22	

V. Conclusion

Modified AUSMPW + /M-AUSMPW+ schemes were presented to solve the ideal MHD equations. To construct AUSMPW + /M-AUSMPW+ appropriate for the ideal MHD equations, the pressure-based weight functions f and w were modified to sense the jumps of magnetic pressure as well as thermal pressure at MHD discontinuities. The modified AUSMPW + /M-AUSMPW+ schemes have the following desirable characteristics in solving the MHD equations.

First, they can remove numerical oscillations effectively behind a strong shock wave. Second, they can guarantee the capture of a stationary contact discontinuity without any numerical dissipation. In addition, the modified M-AUSMPW+ showed enhanced accuracy in a moving contact discontinuity because it was originally designed to minimize numerical dissipation. Third, they were more efficient than a linearized Riemann solver because they did not need the complex eigen-decomposition process of the MHD equations. Through the one-dimensional Ryu and Jones' shock-tube tests, stationary contact tests, and the two-dimensional Orszag–Tang MHD vortex problem, it was confirmed that the modified AUSMPW + /M-AUSMPW+ could solve the complicated physical phenomenon of MHD systems with enhanced accuracy, robustness, and efficiency.

Acknowledgments

This research was supported by National Space Laboratory (NSL: S10801000121-08A0100-12110) program through the Korea Science and Engineering Foundation funded by the Ministry of Education, Science, and Technology. The authors wish to acknowledge this financial support.

References

[1] Yee, K. S., "Numerical Solution of Initial Boundary Value Problems Involving Maxwell's Equations in Isotropic Media," *IEEE Transactions on Antennas and Propagation*, Vol. 14, No. 3, 1966, pp. 302–307.
doi:10.1109/TAP.1966.1138693

[2] Brecht, S. H., Lyon, J. G., Fedder, J. A., and Hain, K., "A Time-Dependent Three-Dimensional Simulation of the Earth's Magnetosphere: Reconnection Events," *Journal of Geophysical Research*, Vol. 87, 1982, pp. 6098–6108.
doi:10.1029/JA087iA08p06098

[3] Evans, C. R., and Hawley, J. F., "Simulation of Magnetohydrodynamic Flows: A Constrained Transport Method," *Astrophysical Journal*, Vol. 332, 1988, pp. 659–677.
doi:10.1086/166684

[4] DeVore, C. R., "Flux Corrected Transport Technique for Multidimensional Compressible Magnetohydrodynamics," *Journal of Computational Physics*, Vol. 92, 1991, pp. 142–160.
doi:10.1016/0021-9991(91)90295-V

[5] Gruber, R., and Rappaz, J., *Finite Element Methods in Linear Ideal Magnetohydrodynamics*, Springer–Verlag, Berlin1985, pp. 79–117.

[6] Salar, N. B., Soulaimani, A., and Habashi, W. G., "A Finite Element Method for Magentohydrodynamics," *Computer Methods in Applied Mechanics and Engineering*, Vol. 190, Nos. 43–44, 2001, pp. 5867–5892.
doi:10.1016/S0045-7825(01)00196-7

[7] Sovinec, C. R., Glasser, A. H., Gianakon, D. C., Barnes, T. A., Nebel, R. A., Kruger, S. E., Schnack, D. D., Plimpton, S. J., Tarditi, A., Chu, M. S., and the NIMROD Team., "Nonlinear Magnetohydrodynamics Simulation Using High-Order Finite Elements," *Journal of Computational Physics*, Vol. 195, March 2004, pp. 355–386.
doi:10.1016/j.jcp.2003.10.004

[8] Brio, M., and Wu, C. C., "An Upwind Differencing Scheme for the Equations of Ideal Magnetohydrodynamics," *Journal of Computational Physics*, Vol. 75, April 1988, pp. 400–422.
doi:10.1016/0021-9991(88)90120-9

[9] Ryu, D. S., and Jones, T. W., "Numerical Magnetohydrodynamics in Astrophysics: Algorithm and Test for One-Dimensional Flow," *Astrophysical Journal*, Vol. 442, March 1995, pp. 228–258.
doi:10.1086/175437

[10] Balsara, D. S., "Total Variation Diminishing Scheme for Adiabatic and Isothermal Magnetohydrodynamics," *The Astrophysical Journal. Supplement Series*, Vol. 116, 1998, pp. 119–131.
doi:10.1086/313092

[11] Dai, W., and Woodward, P. R., "Extension of Piecewise Parabolic Method to Multidimensional Ideal Magentohydrodynamics," *Journal of Computational Physics*, Vol. 115, 1994, pp. 485–514.
doi:10.1006/jcph.1994.1212

[12] Zachary, A., Malagoli, A., and Collela, P., "A High-Order Godunov Method for Multidimensional Ideal Magnetohydrodynamics," *SIAM Journal on Scientific Computing*, Vol. 15, No. 2, March 1994, pp. 263–284.
doi:10.1137/0915019

[13] Aslan, N., "Numerical Solutions of One-Dimensional MHD Equations by a Fluctuation Approach," *International Journal for Numerical Methods in Fluids*, Vol. 22, 1996, pp. 569–580.
doi:10.1002/(SICI)1097-0363(19960415)22:7<569::AID-FLD246>3.0.CO;2-7

[14] Harada, S., Hoffmann, K. A., and Augustinus, J., "Numerical Solution of the Ideal Magnetohydrodynamic Equations of a Supersonic Channel Flow," *Journal of Thermophysics and Heat Transfer*, Vol. 12, No. 4, 1998, pp. 507–513.
doi:10.2514/2.6397

[15] Cargo, P., and Gallice, G., "Roe Matrices for Ideal MHD Systematic Construction of Roe Matrices for Systems of Conservation Laws," *Journal of Computational Physics*, Vol. 136, 1997, pp. 446–466.
doi:10.1006/jcph.1997.5773

[16] Rossmanith, J. A., "An Unstaggered High-Resolution Constrained Transport Method for Magnetohydrodynamic Flows," *SIAM Journal on Scientific Computing*, Vol. 28, 2006, pp. 1766–1797.
doi:10.1137/050627022

[17] Rossmanith, J. A., "A High-Resolution Constrained Transport Method with Adaptive Mesh Refinement for Ideal MHD," *Computer Physics Communications*, Vol. 164, 2004, pp. 128–133.
doi:10.1016/j.cpc.2004.06.020

[18] Steger, J. L., and Warming, R. F., "Flux Vector Splitting of the Inviscid Gasdynamic Equations with Application to Finite-Difference Methods," *Journal of Computational Physics*, Vol. 40, No. , April 1981, pp. 263–293.

[19] Van Leer, B., "Flux-Vector Splitting for the Euler Equation," *Lecture Notes Series*, Vol. 170, No. , 1982, pp. 501–512.

[20] Mignone, A., Bodo, G., Massaglia, S., Matsakos, T., Tesileanu, O., Zanni, C., and Ferrari, A., "PLUTO: A Numerical Code for Computational Astrophysics," *The Astrophysical Journal. Supplement Series*, Vol. 170, 2007, pp. 228–242.
doi:10.1086/513316

[21] Janhunen, P., "A Positive Conservative Method for Magnetohydrodynamics Based HLL and Roe Methods," *Journal of Computational Physics*, Vol. 160, 2000, pp. 649–661.
doi:10.1006/jcph.2000.6479

[22] Linde, T. J., "A Three-Dimensional Adaptive Multifluid MHD Model of the Heliosphere," Ph.D. Dissertation, Aerospace Department, Univ. of Michigan, Ann Arbor, MI, 1998.

[23] Gurski, K. F., "An HLLC-Type Approximate Riemann Solver for Ideal Magnetohydrodynamics," *SIAM Journal on Scientific Computing*, Vol. 25, No. 6, 2004, pp. 2165–2187.
doi:10.1137/S1064827502407962

[24] Li, S., "An HLLC Riemann Solver for Magnetohydrodynamics," *Journal of Computational Physics*, Vol. 203, Feb. 2005, pp. 344–357.
doi:10.1016/j.jcp.2004.08.020

[25] Miyoshi, T., and Kusano, K., "A Multi-State HLL Approximate Riemann Solver for Ideal Magnetohydrodynamics," *Journal of Computational Physics*, Vol. 208, Sept. 2005, pp. 315–344.
doi:10.1016/j.jcp.2005.02.017

[26] MacCormack, R. W., "An Upwind Conservation Form Method for the Ideal Magnetohydrodynamics Equations," *30th Plasmadynamics and Lasers Conference*, AIAA Paper 99-3609, 1998.

[27] Shang, J. S., Canupp, P. W., and Gaitonde, D. V., "Computational Magneto-Aerodynamic Hypersonics," *3rd AIAA Weakly Ionized Gases Workshop*, AIAA Paper 1999-4903, Nov. 1998.

[28] Liou, M. S., "A Sequel to AUSM: AUSM+," *Journal of Computational Physics*, Vol. 129, Dec. 1996, pp. 364–382.
doi:10.1006/jcph.1996.0256

[29] Agarwal, R., and Augustinus, J., "A Comparative Study of Advection Upwind Split (AUSM) and Wave/Particle Split (WPS) Schemes for Fluid and MHD Flows," *30th Plasmadynamics and Lasers Conference*, AIAA Paper 1999-3613, 1999.

[30] Kim, K. H., Kim, C., and Rho, O. H., "Methods for the Accurate Computations of Hypersonic Flows: I. AUSMPW+ Scheme," *Journal of Computational Physics*, Vol. 174, Nov. 2001, pp. 38–80.
doi:10.1006/jcph.2001.6873

[31] Kim, K. H., and Kim, C., "Accurate, Efficient and Monotonic Numerical Methods for Multi-Dimensional Compressible Flows Part I: Spatial Discretization," *Journal of Computational Physics*, Vol. 208, April 2005, pp. 527–569. doi:10.1016/j.jcp.2005.02.021

[32] Tóth, G., "The $\nabla \bullet B = 0$ Constraint in Shock-Capturing Magnetohydrodynamics Codes," *Journal of Computational Physics*, Vol. 161, July 2000, pp. 605–652. doi:10.1006/jcph.2000.6519

[33] Brackbill, J. U., and Barnes, D. C., "The Effect of Nonzero $\nabla \cdot B$ on the Numerical Solution of the Magnetohydrodynamic Equations," *Journal of Computational Physics*, Vol. 35, May 1980, pp. 426–430. doi:10.1016/0021-9991(80)90079-0

[34] Powell, K. G., Roe, P. L., Linde, T., Gombosi, T. I., and De Zeeuw, D. L., "A Solution-Adaptive Upwind Scheme for Ideal Magnetohydrodynamics," *Journal of Computational Physics*, Vol. 154, Sept. 1999, pp. 284–309. doi:10.1006/jcph.1999.6299

[35] Dedner, A., Kemm, F., Kroner, D., Munz, C. D., Schnitzer, T., and Wesenberg, M., "Hyperbolic Divergence Cleaning for the MHD Equations," *Journal of Computational Physics*, Vol. 175, Jan. 2002, pp. 645–673. doi:10.1006/jcph.2001.6961

[36] Lee, Y. J., Munz, C. D., and Schneider, R., "Lagrangian and Symmetry Structure of the Divergence Cleaning Model Based on Generalized Lagrange Multipliers," *International Journal of Modern Physics C*, Vol. 15, No. 1, 2004, pp. 59–114. doi:10.1142/S0129183104005541

[37] Dedner, A., "Solving the System of Radiation Magnetohydrodynamics for Solar Physical Simulations in 3D," Ph.D. Dissertation, Albert-Ludwigs-Universität, Freiburg, Germany, 2003.

[38] Pan, Y., Wang, J. F., and Wu, Y. W., "Upwind Scheme for Ideal 2-D MHD Flows Based on Unstructured Mesh," *Transactions of Nanjing University of Aeronautics & Astronautics*, Vol. 24, No. 1, March 2007, pp. 1–7.

[39] Gurnett, D. A., and Bhattacharjee, A., *Introduction to Plasma Physics*, Cambridge Univ. Press, Cambridge, England, UK, 2005.

[40] Orszag A., and Tang, C. M., "Small-Scale Structure of Two-Dimensional Magnetohydrodynamic Turbulence," *Journal of Fluid Mechanics*, Vol. 90, 1979, pp. 129–143. doi:10.1017/S002211207900210X

[41] Tang, H. Z., and Xu, K., "A High-Order Gas-Kinetic Method for Multidimensional Ideal Magnetohydrodynamics," *Journal of Computational Physics*, Vol. 165, Nov. 2000, pp. 69–88. doi:10.1006/jcph.2000.6597

D. Gaitonde
Deputy Editor